ISSN 1674-1056
http://cpb.iphy.ac.cn
http://iopscience.iop.org/cpb
中国物理 B
Chinese Physics
中国物理 Chinese Physics B

Properties of metal-insulator-metal waveguide loop reflector

Hu Long(龙虎), Xuan-Ke Zeng(曾选科), Yi Cai(蔡懿), Xiao-Wei Lu(陆小微), Hong-Yi Chen(陈红艺), Shi-Xiang Xu(徐世祥), Jing-Zhen Li(李景镇)
Citation: Chin. Phys. B . 2019, 28(9): 094215 . **doi:** 10.1088/1674-1056/28/9/094215
Journal homepage: http://cpb.iphy.ac.cn; http://iopscience.iop.org/cpb

What follows is a list of articles you may be interested in

Geometrical condition for observing Talbot effect in plasmonics infinite metallic groove arrays

Afshari-Bavil Mehdi, Xiao-Ping Lou(娄小平), Ming-Li Dong(董明利), Chuan-Bo Li(李传波), Shuai Feng(冯帅), Parsa Saviz, Lian-Qing Zhu(祝连庆)
Chin. Phys. B . 2018, 27(12): 124204 . **doi:** 10.1088/1674-1056/27/12/124204

Surface plasmon polariton waveguides with subwavelength confinement

Longkun Yang(杨龙坤), Pan Li(李盼), Hancong Wang(汪涵聪), Zhipeng Li(李志鹏)
Chin. Phys. B . 2018, 27(9): 094216 . **doi:** 10.1088/1674-1056/27/9/094216

Plasmonically induced reflection in metal-insulator-metal waveguides with two silver baffles coupled square ring resonator

Zhi-Dong Zhang(张志东), Lian-Jun Ma(马连俊), Fei Gao(高飞), Yan-Jun Zhang(张彦军), Jun Tang(唐军), Hui-Liang Cao(曹慧亮), Bin-Zhen Zhang(张斌珍), Ji-Cheng Wang(王继成), Shu-Bin Yan(闫树斌), Chen-Yang Xue(薛晨阳)
Chin. Phys. B . 2017, 26(12): 124212 . **doi:** 10.1088/1674-1056/26/12/124212

Transmission through array of subwavelength metallic slits curved with a single step or multi-step

Wang Ying-Qi, Wang Yan-Hua, Zheng Xian-Hua, Ye Jia-Sheng, Zhang Yan, Liu Shu-Tian
Chin. Phys. B . 2014, 23(3): 034202 . **doi:** 10.1088/1674-1056/23/3/034202

Enhanced optical transmission by V-shaped nanoslit in metal film

He Meng-Dong, Ma Wang-Guo, Wang Xin-Jun
Chin. Phys. B . 2013, 22(11): 114201 . **doi:** 10.1088/1674-1056/22/11/114201

Properties of metal–insulator–metal waveguide loop reflector*

Hu Long(龙虎)[1,2], Xuan-Ke Zeng(曾选科)[1], Yi Cai(蔡懿)[1], Xiao-Wei Lu(陆小微)[1], Hong-Yi Chen(陈红艺)[1], Shi-Xiang Xu(徐世祥)[1], and Jing-Zhen Li(李景镇)[1,†]

[1] *Shenzhen Key Laboratory of Micro-Nano Photonic Information Technology, College of Electronic Science and Technology, Shenzhen University, Shenzhen* 518060, *China*

[2] *Key Laboratory of Optoelectronic Devices and System of Ministry of Education and Guangdong Province, College of Optoelectronic Engineering, Shenzhen University, Shenzhen* 518060, *China*

(Received 8 April 2019; revised manuscript received 2 July 2019; published online 23 August 2019)

A new type and easy-to-fabricate metal–insulator–metal (MIM) waveguide reflector based on Sagnac loop is designed and investigated. The transfer matrix theoretical model for the transmission of electric fields in the reflector is established, and the properties of the reflector are studied and analyzed. The simulation results indicate that the reflectivity strongly depends on the coupling splitting ratio determined by the coupling length. Accordingly, different reflectivities can be realized by varying the coupling length. For an optimum coupling length of 750 nm, the 3-dB reflection bandwidth of the MIM waveguide reflector is as wide as 1.5 μm at a wavelength of 1550 nm, and the peak reflectivity and isolation are 78% and 23 dB, respectively.

Keywords: surface plasmon polaritons, waveguide, reflector

PACS: 42.82.–m, 42.82.Et, 42.79.Fm **DOI:** 10.1088/1674-1056/ab38a3

1. Introduction

Surface plasmon polaritons (SPPs) are essentially oscillation modes of free electrons coupled with the electromagnetic field at the interface between metallic and dielectric materials.[1] Because they can confine the optical field to the micro-nanometer scale and breakthrough the diffraction limit, SPPs have immense potential to constitute a new generation of all-optical integrated circuits.[2–6] In order to effectively propagate and control SPPs, various SPP waveguides have been studied and designed, including dielectric-loaded waveguides, V-groove waveguides, nanowire waveguides, and metal–insulator–metal (MIM) waveguide.[7,8] Among them, the MIM waveguide can limit the light field at the nanometer scale, which has drawn the attention of researchers. Therefore, devices based on MIM waveguide structures have been proposed, such as couplers, beam splitters, wavelength multiplexers, filters, and reflectors.[9–12] Wherein the reflectors are crucial components in applications such as redirecting SPPs and SPP laser resonators. Therefore, how to obtain reflectors with high-performance and simple structure has become the focus of research.

Currently, different types of SPP reflectors have been developed, including those with a Bragg structure,[13–15] T-shape structure,[16–18] and microcavity structure.[19] For Bragg structure, the reflection can be realized by periodic change of the cladding layer material, the insulator width or material. For example, Ming *et al.* proposed a metal-embedded MIM structure plasmonic Bragg reflector with the transmittance of 86% and filter range from 1.1 μm to 1.3 μm.[13] For T-shape structure, the filters consist of waveguide with a single stub or serial stubs structure. For instance, Liu *et al.* studied the plasmonic reflectors based on serial stub structure with the developed transmission line model.[16] For the microcavity structure, Wang *et al.* studied the flat-top reflection characteristics based on a metal–dielectric–metal (MDM) plasmonic waveguide side coupled with cascaded double cavities.[19] All types of structural filters mentioned above are fabricated the microstructure in or near MIM waveguides. Although those filters have achieved a variety of excellent filtering characteristics, how to fabricate and apply them is still a challenge.

In this study, a new type and easy-to-fabricate MIM waveguide SPP reflector based on Sagnac loop is designed and investigated. The transfer matrix model, used for describing the relationship between the input and output optical fields of each port in the SPP reflector, is established for the first time to our knowledge. The reflection and transmission properties of the reflector are studied and analyzed by combining the transfer matrix model with finite element method (FEM) simulation. Finally, based on the theoretical and simulation results, an optimal SPP reflector is designed to achieve high reflectivity, high isolation, and a large bandwidth simultaneously. This can provide some reference for the research and development of SPP devices.

2. Theoretical model

Figure 1 shows the structure of the MIM waveguide SPP reflector. The metal used is silver and the intermediate insulator layer is poly (methyl methacrylate) (PMMA). The relative

*Project supported by the National Natural Science Foundation of China (Grant Nos. 61827815 and 61775142).

†Corresponding author. E-mail: lijz@szu.edu.cn

© 2019 Chinese Physical Society and IOP Publishing Ltd

permittivities of the silver and PMMA are $\varepsilon_{\rm m}$ and $\varepsilon_{\rm PMMA} = 2.25$, respectively. The width of waveguide is W. The SPPs are coupled to the reflector from port 1 as $\boldsymbol{E}^1_{\rm in}$. Then SPPs enter the coupling region through position 3 after propagating for a distance of 0.8 μm. In the coupling region, t is the separation between the two waveguides and L is the length of the coupling region. The SPPs are split into two beams after passing through the coupling region and they are output from positions 5 and 6. Then, the two beams propagate along a loop with length l and return to the coupling region from positions 6 and 5. Finally, the two beams interfere with each other in the coupling region and are output from port 1 as $\boldsymbol{E}^1_{\rm reflect}$ and port 2 as $\boldsymbol{E}^2_{\rm trans}$. According to the principle of the transfer matrix theory,[20] the theoretical model for the transmission of electric fields in the MIM waveguide reflector can be expressed as follows:

$$\begin{bmatrix} \boldsymbol{E}^2_{\rm trans} \\ \boldsymbol{E}^1_{\rm reflect} \end{bmatrix} = J_{\rm oc} J_{\rm trans} J_{\rm oc} \begin{bmatrix} \boldsymbol{E}^1_{\rm in} \\ 0 \end{bmatrix}, \tag{1}$$

where $\boldsymbol{E}^1_{\rm in}$ and $\boldsymbol{E}^1_{\rm reflect}$ are respectively the input and reflected electric fields from port 1 and $\boldsymbol{E}^2_{\rm trans}$ is the output electric field from port 2. The transmission matrix of the coupling region can be represented as

$$J_{\rm oc} = \sqrt{1-\gamma_{\rm oc}} \begin{bmatrix} \sqrt{1-K} & {\rm i}\sqrt{K} \\ {\rm i}\sqrt{K} & \sqrt{1-K} \end{bmatrix},$$

where i is the imaginary unit, $\gamma_{\rm oc}$ is the coupling loss, and K is the splitting ratio. In general, the phase difference between the two output beams from each arm after passing through the coupling region is $\pi/2$. $J_{\rm trans} = \left[\begin{smallmatrix} 1 & 0 \\ 0 & 1 \end{smallmatrix}\right] \exp[{\rm i}\beta l]$ is the transmission matrix of the loop and $\beta = n_{\rm eff} k_0$ is the propagation constant of the SPP mode in the MIM waveguide, $n_{\rm eff}$ is the effective refractive index, $k_0 = 2\pi/\lambda$ is the vacuum propagation constant, and λ is the wavelength. Based on formula (1), the reflectivity R of port 1 and transmissivity T of port 2 are

$$R = \left| \frac{\boldsymbol{E}^1_{\rm reflect}}{\boldsymbol{E}^1_{\rm in}} \right|^2, \quad T = \left| \frac{\boldsymbol{E}^2_{\rm trans}}{\boldsymbol{E}^1_{\rm in}} \right|^2. \tag{2}$$

The effective refractive index of the SPP mode in the MIM waveguide can be calculated from the dispersion relationship

$$\tanh\left(\frac{1}{2} {\rm d} k_1\right) = -\frac{\varepsilon_{\rm PMMA} k_2}{\varepsilon_{\rm m} k_1}, \tag{3}$$

where k_1 and k_2 are the longitudinal propagation constants in the dielectric and metal, respectively, $k_i = \sqrt{n^2_{\rm eff} k_0^2 - \varepsilon_i k_0^2}$ $(i = 1, 2)$, and d is the thickness of the PMMA layer. The dielectric constant $\varepsilon_{\rm m}$ of silver is obtained using the Drude model:[17] $\varepsilon_{\rm m}(\omega) = \varepsilon_\infty - \omega_{\rm p}^2/(\omega^2 + {\rm i}\omega\gamma)$, where $\varepsilon_\infty = 3.7$ is the interband transition contribution, ω is angular frequency, $\omega_{\rm p} = 1.38 \times 10^{16}$ Hz is the plasmon oscillation frequency of free electrons of the metal, and $\gamma = 2.7 \times 10^{13}$ Hz is the damped oscillation frequency. Formulas (1)–(3) are the transfer matrix model for the propagation of electric fields in the MIM waveguide reflector. Based on this model, the study and analysis of the reflection and transmission properties of a device can be realized via simulation calculation.

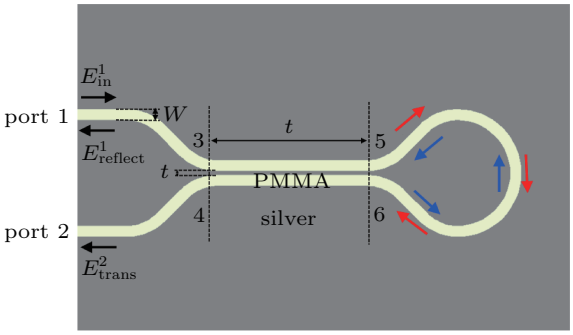


Fig. 1. Structure of the MIM waveguide SPP reflector.

3. Results and discussion

It can be seen from the above theory that the reflectivity of our device is related to the coupling splitting ratio K and the loss $\gamma_{\rm oc}$ of the coupling region. However, the analytical solution for K and $\gamma_{\rm oc}$ is more complicated. Therefore, numerical simulation and analysis combined with finite element method (FEM) are applied to investigate the properties of the coupling region.[21]

When the SPPs are incident from port 1, the variation in the transmissivity of positions 5 and 6 with the coupling length L for different wavelengths of 1 μm, 1.55 μm, and 2 μm is shown in Fig. 2(a), assuming $t = 20$ nm and $W = 50$ nm. As shown in the figure, transmission characteristics exhibit the same trend for different wavelengths. The transmissivity of position 5 tends to decrease initially and then increase periodically as L increases. However, the opposite trend is observed for position 6. Taking the wavelength of 1.5 μm as an example, initially L is 100 nm, which is relatively short, hence most of the power from the SPP input from port 1 is directly output via position 5, and the transmissivity is as high as 88%. Only a small amount of power is coupled to the other branch and output from port 4, and the transmissivity in this case is 4%. The distribution of the absolute value of the electric field ($|\boldsymbol{E}|$) in the waveguide coupler is shown in Fig. 2(b). As is shown, the SPPs are mostly output from position 5. When $L = 750$ nm, the transmissivities of positions 5 and 6 are equal, and the corresponding electric field distribution is shown in Fig. 2(c), which indicates that a 50:50 splitting ratio is realized at this coupling length. For $L = 1.5$ μm, the electric field distribution is shown in Fig. 2(d), and the transmissivity of position 6 reaches a maximum of 84%, while that of position 5 is 0.5%. However, the minimum transmissivity of position 5 does not occur at $L = 1.5$ μm, but at $L = 1.6$ μm, which is $\sim 0.1\%$. The different L values corresponding to the extreme values

of transmissivity for each port are attributed to the additional phase introduced by the imaginary part of the dielectric constant of the metal.[21] Owing to the transmission loss of SPPs, the transmissivity of the two ports is gradually reduced as the length of the coupling region increases. In order to reduce the loss, the required splitting ratio K is generally selected in the first period. The coupling splitting ratio can be calculated based on the results shown in Fig. 2. In addition, γ_{oc} can be deduced from the relationship between amplitude reduction and length increase. Although the transmission characteristics exhibit the same trend, the coupling strengths for different wavelengths are different, resulting in transmissivities of position 5 and position 6 at the same coupling length. For instance, the 50:50 splitting ratio is realized at the short coupling length of 400 nm for the wavelengths of 1 μm, however, for the wavelengths of 2 μm, the coupling length increases to 1 μm to achieve the same splitting ratio. It can be seen that the SPPs with short wavelength can achieve strong coupling at a short coupling length. Moreover, the properties of the coupling region are affected by the waveguide separation distance and the smaller the value of t, the stronger the coupling effect.[21,22] The theoretical analysis of the MIM waveguide reflector can be realized by applying K and γ_{oc} to the transfer matrix model, as described in formula (1).

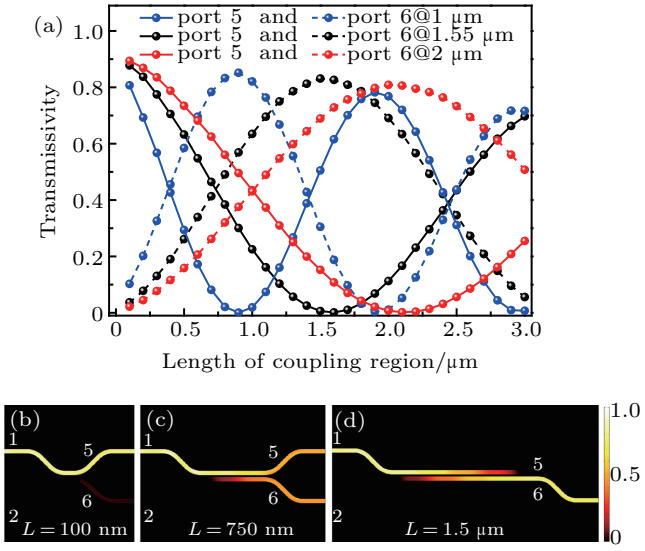


Fig. 2. (a) Variation of the transmissivity of positions 5 and 6 over the coupling length L when $t = 20$ nm for the wavelengths of 1 μm, 1.55 μm, and 2 μm; Distribution of the absolute value of the electric field ($|\boldsymbol{E}|$) at each port under the coupling length of (b) 100 nm, (c) 750 nm, and (d) 1.5 μm for $\lambda = 1.55$ μm.

Without loss of generality, the wavelength of 1.5 μm and $l = 2$ μm is chosen and the reflection and transmission characteristics of the device are investigated. The variation curves of reflectivity R of port 1 and transmissivity T of port 2 in the MIM reflector over the coupling length L calculated using both the transfer matrix model and FEM are shown in Fig. 3(a).

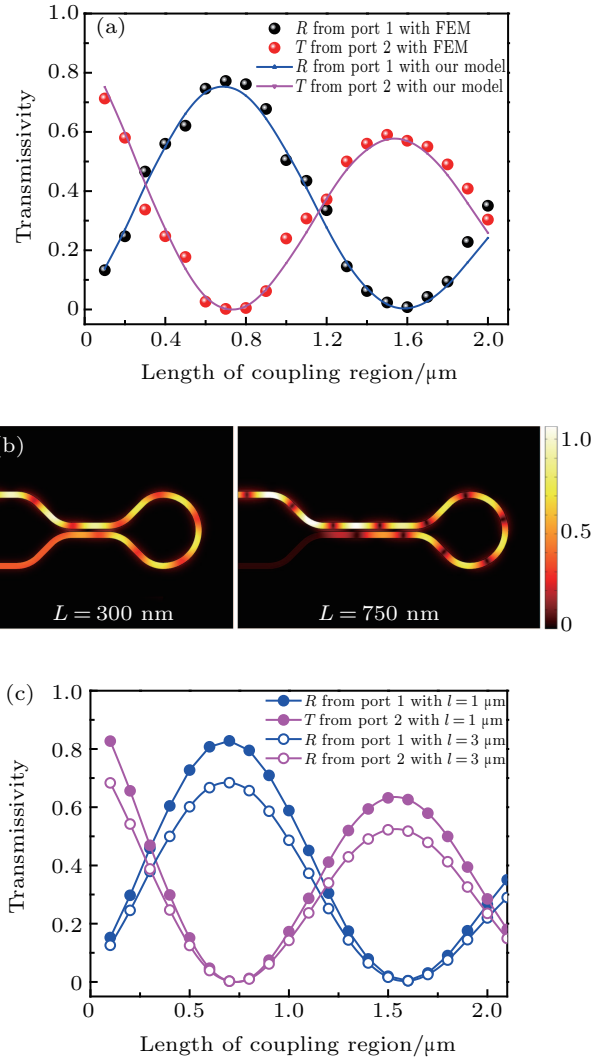


Fig. 3. (a) Variation of reflectivity of port 1 and transmissivity of port 2 over the coupling length L when the wavelength is 1.55 μm and $l = 2$ μm (points for the transfer matrix model results; lines for the FEM results); (b) Distribution of the absolute value of the electric field in the reflector under L of 300 nm and 750 nm when $l = 2$ μm; (c) Variation of reflectivity of port 1 and transmissivity of port 2 for $l = 1$ μm and $l = 3$ μm.

As shown in the figure, both R and T tend to vary periodically and alternately as L increases. When $L = 300$ nm, the splitting ratio of ports 3 and 4 is 77:13 (shown in Fig. 2(a)), and the reflectivity equals transmissivity, indicating that the reflection with 50% is achieved at this coupling length. The left image in Fig. 3(b) shows the distribution of a normalized electric field of the reflector. The light and dark fringes of the electric field of SPPs are observed in the device, indicating that the electric fields in both directions interfere. And for $L = 750$ nm, R reaches a maximum of 78% when T is approximately 0.4% as shown in Fig. 3(a), corresponding to an extinction ratio of 23 dB. At this length, the coupling region realizes a 50:50 splitting ratio. The right image in Fig. 3(b) shows the distribution of a normalized electric field. As is shown in the figure, there is a very obvious interference phenomenon in the device, and the light input to port 1 is completely output from port 1 after propagating through the device, which demonstrates its function of total reflection. It can be seen

that the reflection and transmission characteristics of the device strongly depend on the coupling splitting ratio, while the splitting ratio in turn depends on the coupling length. Reflectivity can be varied by changing the coupling length. When the splitting ratio is 50:50, the strongest interference condition is observed, and the total reflection can be achieved. In addition, figure 3(a) shows that the results obtained from the transfer matrix model and FEM simulation agree well in spite of small discrepancies caused by the reflection of the boundary condition in the FEM simulation. This confirms the accuracy of our proposed theoretical model. In addition, the length of the loop also affects the reflection and transmission characteristics of the device. Figure 3(c) shows the variation of reflectivity in the port 1 and transmissivity of port 2 for $l = 1$ μm and 3 μm. It can be seen from the figure that the change in length l does not affect the overall trends of R and T, but affects the amplitudes of R and T due to different losses. The short length helps reduce the loss, and the transmittance and reflectivity are improved. However, the length cannot be reduced directly because the bending loss increases when the length reduces to a certain level, therefore the length of the loop must be optimized.

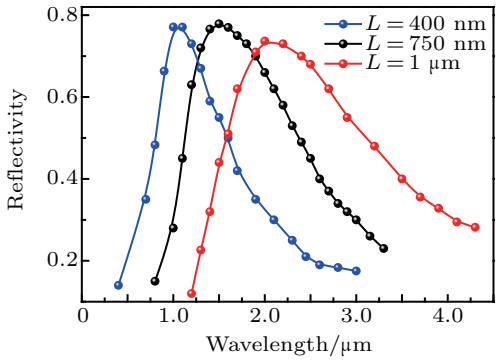


Fig. 4. Simulation results of reflectivity under different wavelengths of incident light when $L = 400$ nm, 750 nm, and 1 μm.

The simulation results of the reflectivity of the device for different wavelengths λ of the incident light when L is 400 nm, 750 nm, and 1 μm are shown in Fig. 4. It can be seen that the reflectivity initially increases and then decreases as the wavelength increases for all coupling lengths. However, the peak position and bandwidth of the reflectivity are different for different coupling lengths. When $L = 400$ nm, because a 50:50 splitting ratio is realized when the wavelength is 1 μm (shown in Fig. 2(a)), the reflectivity reaches its maximum at $\lambda = 1$ μm, and the 3-dB reflection bandwidth is 0.97 μm. And for $L = 750$ nm and 1 μm, the peak positions shifts to 1.55 μm and 2 μm, and the reflection bandwidth has been extended to 1.5 μm and 2 μm, respectively. Therefore, it is necessary to design the length of the coupling region according to the interesting wavelength, and the shorter wavelength has a narrower bandwidth.

4. Conclusion

A new type and easy-to-fabricate metal–insulator–metal waveguide reflector based on Sagnac loop was designed and investigated. The transfer matrix theoretical model for the transmission of electric fields in the reflector was established for the first time and the properties of the reflector were studied and analyzed. The simulation results indicate that the reflectivity of the reflector strongly depends on the coupling splitting ratio determined by the coupling length. For an optimum coupling length of 750 nm when the wavelength is 1.55 μm, the reflectivity and isolation were 78% and 23 dB, respectively. Moreover, the peak position and bandwidth of the reflection spectrum also varied with the coupling length. For a larger coupling length becomes longer, the peak position became to longer wavelengths and the bandwidth became wider.

References

[1] Raether H 1988 *Surface plasmons on smooth and rough surfaces and on gratings* (Heidelberg: Springer, Berlin)
[2] Barnes W L, Dereux A and Ebbesen T W 2003 *Nature* **424** 824
[3] Li S, Wang Y, Jiao R, Wang L, Duan G and Yu L 2017 *Opt. Express* **25** 3525
[4] Wang Y, Li S, Zhang Y and Yu L 2016 *IEEE Photonics J.* **8** 1
[5] Chen J, Li Z, Zou Y, Deng Z and Xiao J 2013 *Plasmonics* **8** 1627
[6] Yang L, Li P, Wang H and Li Z 2018 *Chin. Phys. B* **27** 094216
[7] Berini P and De Leon I 2012 *Nat. Photon.* **6** 16
[8] Yao J, Wei Q, Ma Q Y and Wu D 2017 *Chin. Phys. B* **26** 057302
[9] Shin Y J, Son J H, Lee D H and Lee M H 2017 *J. Nanosci. Nanotechnol.* **17** 7093
[10] Wang G, Lu H, Liu X, Mao D and Duan L 2011 *Opt. Express* **19** 3513
[11] Zhao S, Zhang H C, Zhao J and Tang W X 2017 *Sci. Rep.* **7** 10576
[12] Chen J, Yang J, Chen Z, Fang Y J, Zhan P and Wang Z L 2012 *AIP Adv.* **2** 012145
[13] Tian M, Lu P, Chen L, Liu D and Peyghambarian N 2012 *Opt. Commun.* **285** 5122
[14] Gong Y, Wang L, Hu X, Li X and Liu X 2009 *Opt. Express* **17** 13727
[15] Davoodi F and Granpayeh N 2019 *Opt. Quantum Electron.* **51** 9
[16] Liu J, Fang G, Zhao H, Zhang Y and Liu S 2009 *Opt. Express* **17** 20134
[17] Lin X S and Huang X G 2008 *Opt. Lett.* **33** 2874
[18] Shen X, Wang Y, Yan X, Yuan L and Sang T 2016 *Appl. Opt.* **55** 6443
[19] Wang S, Xu Y, Lan S and Wu L 2011 *Plasmonics* **6** 689
[20] Mortimore D B 1988 *J. Lightwave Technol.* **6** 1217
[21] Han Z, Liu L and Forsberg E 2006 *Opt. Commun.* **259** 690
[22] Gramotnev D K, Vernon K C and Pile D F P 2008 *Appl. Phys. B: Lasers Opt.* **93** 99